THE JOURNAL OF PHYSICAL CHEMISTRY C

Article

pubs.acs.org/JPCC

MoS_2 Quantum Dot: Effects of Passivation, Additional Layer, and *h*-BN Substrate on Its Stability and Electronic Properties

G. C. Loh,*[,†,‡] Ravindra Pandey,*[,†] Yoke Khin Yap,[†] and Shashi P. Karna[§]

[†]Department of Physics, Michigan Technological University, Houghton, Michigan 49931, United States

[‡]Institute of High Performance Computing, 1 Fusionopolis Way, #16-16 Connexis, Singapore 138632, Singapore

[§]U.S. Army Research Laboratory, Weapons and Materials Research Directorate, ATTN: RDRL-WM, Aberdeen Proving Ground, Maryland 21005-5069, United States

Supporting Information

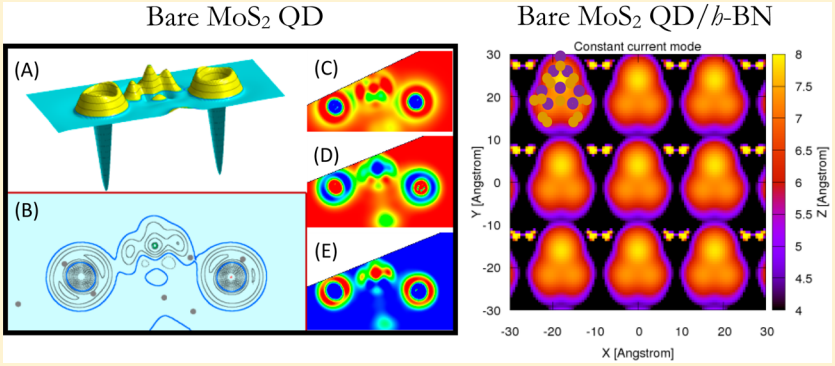

ABSTRACT: The inherent problem of a zero-band gap in graphene has provided motivation to search for the next-generation electronic materials including transition metal dichalcogenides, such as MoS_2. In this study, a triangular MoS_2 quantum dot (QD) is investigated to see the effects of passivation, additional layer, and the *h*-BN substrate on its geometry, energetics, and electronic properties. The results of density functional theory calculations show that the monolayer QD is metallic in nature, mainly due to the coordinatively unsaturated Mo atoms at the edges. This is reaffirmed by the passivation of the S edge atoms, which does not significantly modify its metallic character. Analysis of the chemical topology finds that the Mo−S bonds associated with the edge atoms are predominantly covalent despite the presence of metallic states. A bilayer QD is more stable than its monolayer counterpart, mainly due to stabilization of the dangling bonds of the edge atoms. The degree of the metallic character is also considerably reduced as demonstrated by the *I*−*V* characteristics of a bilayer QD. The binding strength of a monolayer QD to the *h*-BN substrate is predicted to be weak. The substrate-induced modifications in the electronic structure of the quantum dot are therefore not discernible. We find that the metallic character of the QD deposited on the insulating substrate can therefore be exploited to extend the functionality of MoS_2-based nanostructures in catalysis and electronics applications at the nanoscale level.

1. INTRODUCTION

Two-dimensional (2D) transition metal dichalcogenides (TMDs) are a novel category of materials that has drawn a notable amount of interest. One such material is molybdenum disulfide (MoS_2), which has unique, intriguing, and yet functional properties, including a large carrier mobility[1] and high current-carrying capacity.[2] Akin to many other TMDs, the electronic band structure of MoS_2 is contingent on the number of layers; it is a semiconductor with a direct band gap between 1.58 and 1.87 eV[3−5] in the monolayer, and the band gap becomes indirect with the value of 1.3 eV[6,7] in the bulk form. Therefore, the few-layer MoS_2 is not preferred in optoelectronic applications, while it is still favorable for electronic devices.

The MoS_2 monolayer is stacked in the so-called S−Mo−S sandwich-like arrangement, with Mo atoms being trigonal and prismatic with respect to S atoms. Unlike its close relative graphene, the MoS_2 monolayer is noncentrosymmetric, and only exhibits inversion symmetry in bilayers or the bulk configuration. The intralayer Mo−S bonds are covalent, while the interaction between layers in multilayer MoS_2 is of the van der Waals (vdW) type. The relative weak interlayer forces allow the existence of different polytypes of MoS_2 including its orthogonal variant.[8−10] The spin-splitting at the valence-band maximum (VBM) and the presence of conduction and valence band valleys in their band structures also make MoS_2 suitable for spin-[11] and valley-tronics devices.[11,12]

Currently, MoS_2 sheets can be attained primarily by two methods: (1) micromechanical cleavage or exfoliation of bulk crystals,[13] and (2) growth using chemical vapor deposition

Received: October 21, 2014
Revised: December 22, 2014
Published: December 23, 2014

DOI: 10.1021/jp510598x
J. Phys. Chem. C 2015, 119, 1565−1574

(CVD).[14−18] In the former method, cleavage often results in thin films that are small in area (i.e., quantum dots), contain topological defects such as impurities, and consist of more than one layer. Likewise, MoS_2 grown by the CVD process is also adversely affected by defects due to imperfection induced by the growth conditions.[19,20] Synthesis begins with the nucleation of Mo and S atoms at numerous sites on the substrate. These nuclei or islands subsequently grow as more atoms bond to them, and they eventually meet one another, forming a film with misoriented grains.[15,16] However, in many instances, instead of continuous films, nanocrystallites of well-defined shapes with sharp straight edges are observed.[21,22] It was theoretically speculated that the MoS_2 islands could exist in different shapes (such as trigonal, hexagonal, truncated hexagonal, and rhombohedral), but in experiments, only the triangular ones were observed,[23−26] with dimensions in tens to hundreds of nanometer. It is also suggested that the triangularity of the quantum dots demonstrates the 3-fold symmetry, and hence the monocrystallinity of the material.[21]

Apparently, the shape of MoS_2 plays a vital role in device performance. Size is another crucial factor; when a material is downscaled to an extent such that its structural dimension is comparable to or below that of its electron wave function, quantum confinement is observed.[27] In this context, reducing a sheet to the nanometer size essentially transforms it into a quantum dot (QD). How do quantum mechanical effects modulate the geometry, energetics (such as formation energy), and other electronic characteristics (such as charge density, spin density) of MoS_2? Moreover, are these properties layer-dependent; that is, does a monolayer QD behave similarly to its bilayer counterpart? In what ways will these properties modify when the QD is deposited on an electrically insulating material such as hexagonal BN (*h*-BN)? In this study, we examine such questions in detail with density functional theory for the triangular MoS_2 QDs. To attenuate the quantum mechanical effects, we passivate the edge S atoms of QD by hydrogen (H), and investigate the effects of passivation on the aforementioned properties. Last but not least, the effects of dangling bond states on chemical topology of the QD are investigated using the quantum theory of atoms in molecules (QTAIM).[32−36] Note that physics and chemistry of such stoichiometric MoS_2 QDs have not yet been studied, although sulfur-excess MoS_2 nanostructures including clusters, flakes, and platelets were the focus of both experimental and theoretical studies.[23,26,28−31]

2. COMPUTATIONAL MODEL

We employ a supercell model in which the basic configuration consists of an isosceles triangular MoS_2 QD, with its surface parallel to the (001) plane (Figure 1a). We define the point opposite the base of the isosceles triangle as the "head", while the base is the "tail". The length of the QD in the direction of the longest dimension, that is, from head to tail, is approximately 11 Å for the QD consisting of 8 "formula units" of MoS_2, that is, 8 Mo atoms and 16 S atoms in the supercell. The *h*-BN substrate is simulated by a (7×7) BN unit cell consisting of 98 atoms (i.e., 49 B and 49 N atoms), on top of which the MoS_2 QD is deposited. To provide a more comprehensive picture of the QD, we have performed multislice simulations[37,38] to calculate its TEM (transmission electron microscopy), HA-ADF (high-angle annular dark-field), and BF-STEM (bright-field scanning transmission electron microscopy) images together with its average (*Z*-number × Debye−Waller factor)^2 plot (Figure 1b−e). There is a palpable difference between the image contrast at the Mo and S atoms.

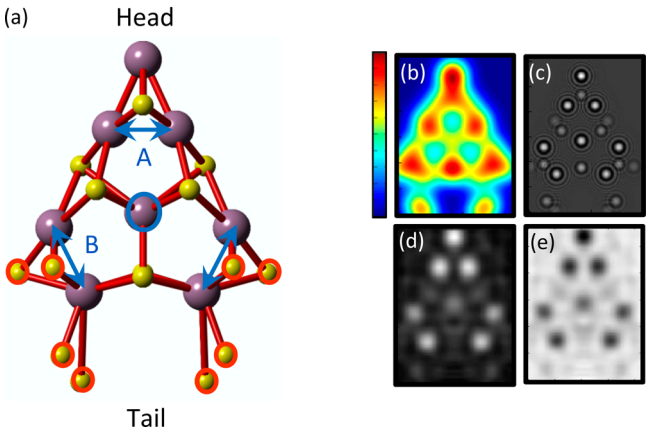

Figure 1. (a) Triangular monolayer MoS_2 QD where coordinatively unsaturated S atoms are shown by the red circles. Atoms in purple are Mo, and yellow are S. Multislice simulations: (b) simulated average (*Z*-number × Debye−Waller factor)^2 plot (the color bar denotes the magnitude in arbitrary units), (c) simulated TEM image, (d) simulated HA-ADF image, and (e) simulated BF-STEM image. In (a), the blue arrows refer to the Mo−Mo distances given in Table 1. The labels A and B refer to the two different pairs of Mo atoms of the QD. The blue circle marks the central Mo atom above which the STM tip is positioned as discussed in section 6.

Calculations based on density functional theory (DFT) were performed with the VASP (Vienna Ab Initio Simulation Package) package, and the implementation of projector augmented-wave (PAW) pseudopotentials[39] (with an energy cutoff of 400 eV). The Perdew−Burke−Ernzerhof (PBE) exchange-correlation functional in the generalized gradient approximation (GGA)[40] was used. Dispersion correction was included in the calculations by the DFT-D2 approach of Grimme.[41] The Brillouin zone was sampled with a $(9 \times 9 \times 1)$ *k*-point mesh using the Monkhorst−Pack scheme.[42] The structures were optimized until the forces (as calculated by the Hellmann−Feynman formalism[43,44]) were less than 10^{-5} eV/Å. In the supercell, the structure is separated from its periodic image in the direction perpendicular to the surface by a vacuum region of 10 Å. Dipole corrections were applied in the direction perpendicular to the material surface to avoid interactions between periodically repeated images.

To partition the continuous charge density among the atoms in the system, Bader's atoms in molecules theory[32−36] is implemented, such that the atomic basin is determined at the zero flux surface around the atom. This surface is observed in the two-dimensional sense at which the charge density is at a minimum perpendicular to the system surface. Therefore, the total electronic charge of each atom can be defined.

3. MoS_2 MONOLAYER QD: BARE AND PASSIVATED

Because of the cleaving of the MoS_2 monolayer into a triangular QD, dangling bonds (or free radicals) at the edges of the QD are created. The triangular QD shown in Figure 1 consists of 5 under-coordinated Mo and 8 under-coordinated S atoms. To examine the effects of the dangling bond states on the intrinsic electronic structure of the QD,[45] passivation by H atoms is implemented in two ways: (i) partial passivation of the under-coordinated S atoms, referred to as partially (S) passivated (marked by red circles in Figure 1), and (ii) full passivation of

DOI: 10.1021/jp510598x
J. Phys. Chem. C 2015, 119, 1565−1574

all S atoms, referred to as fully (S) passivated. Note that infrared spectroscopy measurements have indicated the presence of S−H groups at the edges of MoS_2 clusters.[46] In both partially and fully passivated cases, the edge Mo atoms are coordinatively unsaturated. Although it has been reported[24,25] that the Mo edges with unsaturated dangling bonds in a bare QD may not be stable, our results based on the Mo_nS_{2n} configuration find the bare stoichiometric QD to be stable.

Modifying the dimensions of a nanostructure alters its surface energy and consequently changes its molecular geometry. As the distribution of electrons is inherently dependent on the bonding characteristics of a nanostructure, reducing the size of a 2D sheet such as MoS_2 to a QD inevitably modifies its charge density distribution. The charge density plots indicate substantial interaction between the Mo atoms of the bare MoS_2 QD (top panel of Figure 2). In the middle panel

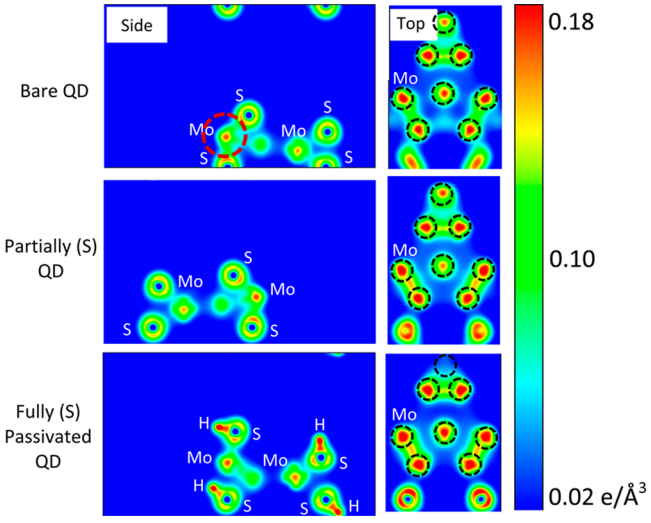

Figure 2. Charge density plots of bare, partially (S) passivated QD, and fully (S) passivated monolayer MoS_2 QD. The left panel is the side view taken through the central plane passing through Mo atom at the head of the QD. The right panel is the top view taken through the plane consisting of Mo atoms. The black dashed circles show the position of the Mo atoms.

of Figure 2, H atoms are not visible because the 2D plane is taken through the center of the QD. In both partially and fully (S) passivated QDs, the charge density between some Mo pairs (represented in orange) is significantly greater than that between the corresponding Mo pair in the bare QD (in green). In addition, the charge density between H and S atoms in the fully (S) passivated QD is relatively large with respect to that in the neighboring region.

Table 1 lists the distance (R) between the pairs of Mo atoms (e.g., A and B of Figure 1) for the equilibrium configurations of the QDs, sheet, and bulk MoS_2. Both $R_{(Mo-Mo(A))}$ and $R_{(Mo-Mo(B))}$ of the MoS_2 QD are significantly smaller than the corresponding values in the MoS_2 monolayer, indicating a contraction of bonds due to surface energy as described by the bond-order-length-strength (BOLS) correlation.[47−49] The bond contraction is affirmed in the charge density plots (Figure 2) indicating a relatively strong interaction between some of the Mo atoms. H passivation further reduces the Mo−Mo distances in the QD. The structural stability of the QD is expressed by the formation energy (Figure S1, Supporting Information), which is defined as the difference between the total energy of the system and the sum of the energy of its constituents:

$$E_f = E_{MoS2} - \sum_{\alpha=Mo,S} n_\alpha E_\alpha \quad (1)$$

where E_{MoS2} is the total energy of the QD, n_α is the number of atoms of a particular element α, and E_α is the energy of a single atom of that element α.

The stability of the QD depends on the degree of H passivation of the S atoms; the calculated formation energy is −5.89, −5.37, and −4.85 eV/atom for the bare, partially, and fully passivated QDs, respectively, which is comparable in its order of magnitude to that of 1H-MoS_2 monolayer (∼5.18 eV/atom),[3] and that of Mo_nS_{2n+x} clusters (∼5 eV/atom).[26]

By using Bader's method to draw the atomic boundaries,[32−36] the on-site charges are computed, and the changes in their values with respect to the intrinsic values are shown in Figure S1 (Supporting Information). The Mo atoms lose electrons, while the S atoms gain electrons in the bare QD. This is complemented by (i) Figure 3, which plots the charge transfer within each QD, and (ii) the magnitude of electronegativity of Mo (2.16) and S (2.58) in the Pauling scale.[50]

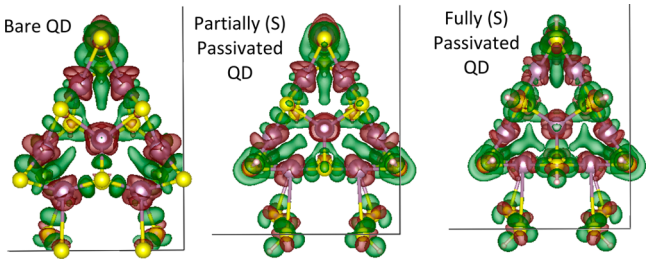

Figure 3. Top views of the charge transfer landscape of bare, partially (S) passivated QD, and fully (S) passivated monolayer QD. The contour isovalue is 0.002 e/Å^3. Green, accumulation region; purple, depletion region.

The chemical bond, or more specifically the electron density distribution between atoms, can be described by the Laplacian of the electron density via the quantum theory of atoms in molecules[32−36] (see the Supporting Information). In Bader's theory, the covalency of the bonds is expressed by (1) the form

Table 1. Calculated Bond Distance between Mo Atoms (As Marked in Figures 1 and 2) in Bare Monolayer QD, Partial (S) Passivated Monolayer QD, Fully (S) Passivated Monolayer QD, Bare Bilayer QD, Monolayer Sheet, and Bulk MoS_2[a]

	bare monolayer QD	partially (S) passivated monolayer QD	fully (S) passivated monolayer QD	bare bilayer QD	monolayer sheet	bulk
$R_{(Mo-Mo(A))}$ (Å)	2.20	2.17	2.17	2.53	3.22	3.22
$R_{(Mo-Mo(B))}$ (Å)	2.37	2.07	2.07	2.76	3.22	3.22
interlayer distance (Å)	1.38	1.44	1.51	1.79	1.55	1.54

[a]The average interlayer distance is derived by computing the average distance between each sublayer.

DOI: 10.1021/jp510598x
J. Phys. Chem. C 2015, 119, 1565−1574

of the zero envelope of the negative Laplacian, and (2) the value of the negative Laplacian at the bond critical point (bcp).

To study the effects of dangling bond states on the chemical topology in the bare QD, we consider the head, midsection, and tail of the QD, because the apex Mo atom at the head and the two S atoms at the tail are strongly under-coordinated, while the atoms at the midsection are fully coordinated. Figure 4 shows (A,B) the negative Laplacian plots, (C) the kinetic

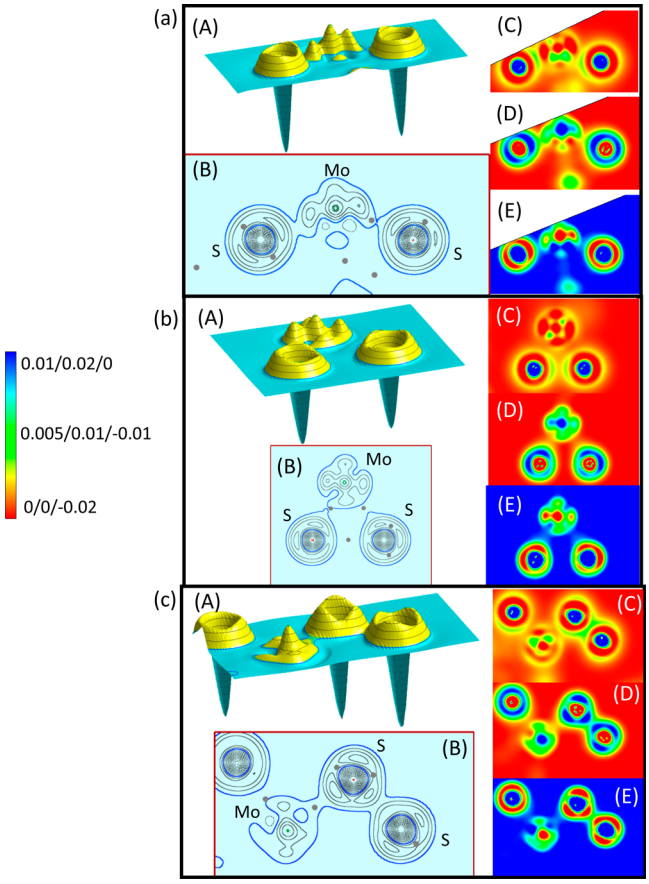

Figure 4. Bare MoS_2 QD: (A) 3D negative Laplacian plot, (B) 2D negative Laplacian plot, (C) kinetic energy density, (D) potential energy density, and (E) electronic energy density of (a) head, (b) midsection, (c) tail. The green and red lines in the 2D negative Laplacian plots represent the maxima and minima of electron density, respectively. The color bar shows the energy density in $E_h a_0^{-3}$, whereby E_h is hartree and a_0 is Bohr radius, with the numerals in the scale for the kinetic, potential, and electronic energy densities, respectively.

energy density, (D) the potential energy density, and (E) the electronic energy density of the bare QD, whereas Supporting Information Figure S2 shows that of the passivated QD. As the plane taken through the Mo and S atoms at the tail does not slice through the H atoms that are bonded to the S atoms, the H atoms are not visible in Supporting Information Figure S2(c). The gray dots represent the bcp in the charge profile. It is evident that the covalency varies at different regions of the QD. The Mo−S bonds at the head and tail of the bare QD are predominantly covalent, because the zero envelope of the negative Laplacian surrounds the bcp.

On the other hand, the Mo−S bonds at the midsection are primarily ionic. With H-passivation of the edge S atoms, these bonds become more ionic in nature. The bond charge concentration (BCC) in the passivated QD is of lower magnitude than that in the bare QD, due to the sharing of charges with the H atoms. Moreover, the electronic energy density plots (E) complement the 2D and 3D negative Laplacian plots by reflecting the covalency of the interaction between the atoms; the electronic energy density decreases with the covalency of the bond. The electronic energy density between the Mo and S atoms in the nonpassivated QD is slightly greenish-blue (Figure 4), while it is dark blue in the passivated QD. This suggests that the covalency of the Mo−S bond is greater in the bare QD. As a comparison, the electronic energy density between the H and S atoms in the passivated QD is much smaller (in red), implying a more covalent bond between the constituent atoms.

Figure 5 shows the calculated projected atomic density of states (DOS) to characterize the nature of the energy bands of

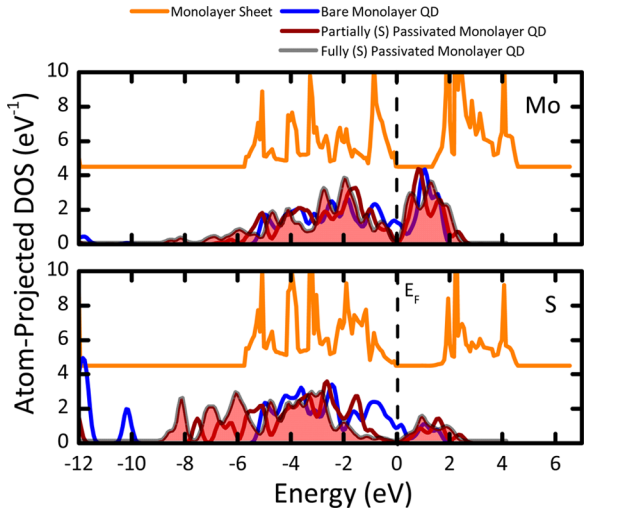

Figure 5. Atom-projected density of states of a monolayer sheet, bare monolayer QD, partially (S) passivated monolayer QD, and fully (S) passivated monolayer QD. Zero is taken to be the Fermi energy of the QD. For the monolayer sheet, the origin of DOS is shifted upward for clarity.

the QD. It also includes DOS of the monolayer indicating its band gap to be about 1.6 eV, which is in close agreement with previously reported DFT values.[3−7,51] Reduction of the monolayer sheet into QD transforms it to become metal-like with the presence of states associated with both Mo and S atoms at the Fermi level. This is coherent with previous reports performed on nonstoichiometric S-excess MoS_2 nanoclusters and nanoplatelets.[23,26,28−31] Passivation of S atoms reduces the hybridization between Mo and S states, and leads to a decrease in the magnitude of DOS at the Fermi level due to saturation of the dangling bonds at edge atoms. However, it is still nonzero because passivation of S atoms unambiguously draws out contributions of Mo states at the Fermi level.

To investigate the preferred spin states of the MoS_2 QDs in the equilibrium configuration, we begin with the calculation by considering the QD to be in the nonmagnetic, ferromagnetic (FM), and antiferromagnetic (AFM) spin configurations. In the nonmagnetic state, the spin moment of each atom is initialized to be zero. On the other hand, FM and AFM spin states consist of parallel (↑↑) and antiparallel (↑↓) spins of neighboring atoms, respectively. Figure 6a illustrates the spin density distribution in the equilibrium configuration of a bare MoS_2

DOI: 10.1021/jp510598x
J. Phys. Chem. C 2015, 119, 1565−1574

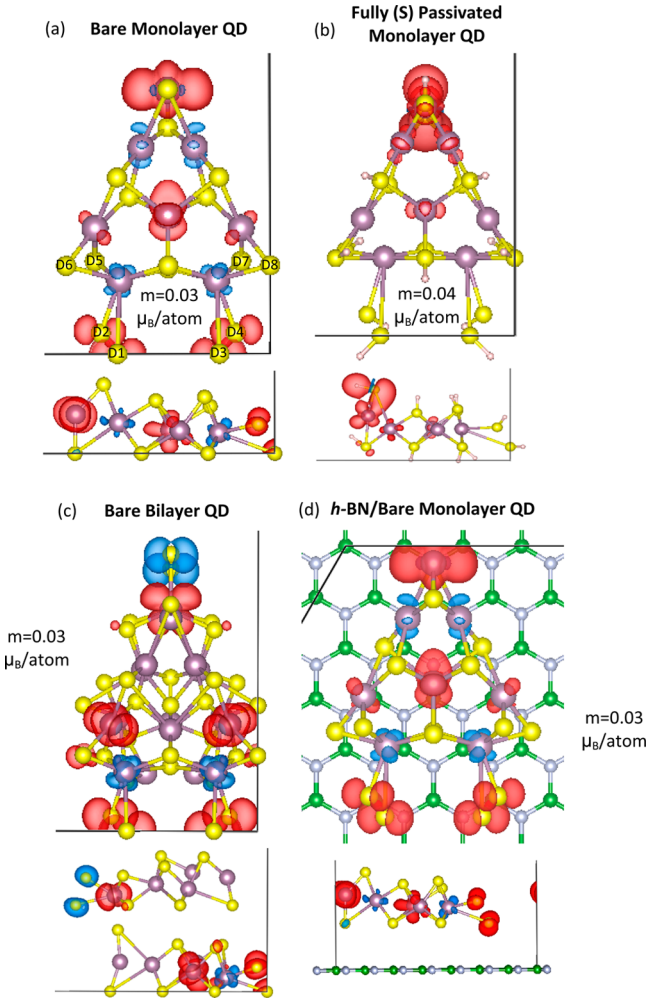

Figure 6. Spin density distribution in the equilibrium configurations of (a) bare monolayer QD, (b) fully (S) passivated monolayer QD, (c) bare bilayer QD, and (d) bare monolayer MoS_2 QD deposited on a *h*-BN substrate. The contour isovalue is 0.002 e/Å^3. Regions in red have a net spin-up density, whereas those in blue have a net spin-down density. The average magnetization moment is shown. In (a), D1−D8 denote S atoms that are coordinatively unsaturated.

QD; the regions in red have a larger spin-up density (i.e., $n_{up} - n_{down} > 0$), while those in blue have a larger spin-down density (i.e., $n_{up} - n_{down} < 0$).

In the bare QD, the Mo atoms are AFM-coupled. The electron spin density is predominantly uniform, and there is no preferential accumulation of either type of electrons at Mo or S atoms. Note that the difference in total energy of the nonmagnetic and AFM spin configurations is less than 0.002 eV, well within the accuracy of our model. We therefore consider the nonmagnetic and AFM spin configurations to be degenerate for the bare QD. On the other hand, a fully (S) passivated QD induces a redistribution of the electron spin, and the spin-up states are concentrated at the head of the QD (Figure 6b). The magnetization moment increases slightly from 0.03 to 0.04 μ_B/atom. In contrast, partially passivation induces spin redistribution in such a way that essentially reduces the moment to zero. Figure S3 (Supporting Information) shows the spin-polarized orbital-projected density of states for each constituent atom. There is a slight difference in the Mo d-orbital states (as marked by arrow), justifying the minute magnitude of the magnetization moment in the bare QD.

4. BILAYER MoS_2 QD

To investigate the layer-dependence of the electronic properties, the monolayer QD is extended to the bilayer form by cleaving a MoS_2 bilayer sheet into a bilayer QD consisting of two stacked isosceles triangular QDs. The layers are stacked in such a way that the head of each QD faces opposite directions. Figure 7 shows the equilibrium configuration of the bilayer QD.

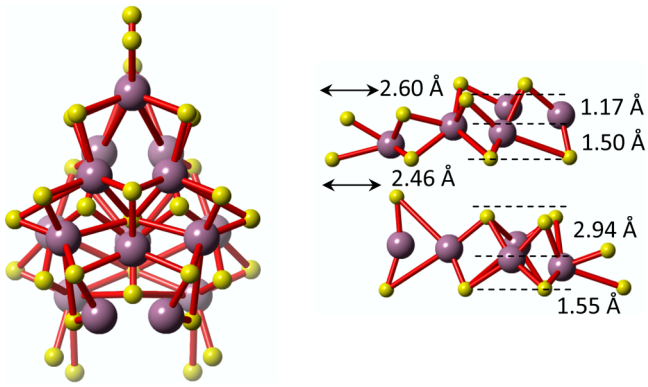

Figure 7. Top and side views of a bare bilayer MoS_2 QD. The intra- and interlayer geometry is depicted in the bottom panel.

The supercell is made up of 16 "unit cells" of MoS_2, 8 Mo atoms and 16 S atoms form each stacked layer. $R_{(Mo-Mo(A))}$, $R_{(Mo-Mo(B))}$, and average interlayer distances are given in Table 1. The Mo−Mo distance is intermediate between that of the monolayer QD and the monolayer sheet. Its average interlayer distance is larger than that of its monolayer sheet, and the formation energy (eq 1) is calculated to be −5.95 eV/atom. The slightly increased structural stability of a bilayer QD might be effectuated by the van der Waals interaction, which stabilizes the edge atoms with dangling bonds.[52,53]

The charge density landscape of the bare bilayer MoS_2 QD is shown in Figure 8a. The electron density between some of the Mo atoms is significantly large, mirroring that noted in Figure 2. Although the Mo−$Mo_{(A)}$ and Mo−$Mo_{(B)}$ distances are about 15% larger than those in the monolayer QD, they are still relatively small as compared to those of the monolayer sheet. The total DOS of the Mo and S atoms in the bare monolayer and bare bilayer QDs are presented in Figure 8b. There is a large reduction in the number of occupied states in the bilayer QD near the Fermi level, which could be due to suppression of the electron mobility by vdW interaction between neighboring S atoms on opposite layers in the bilayer QD, thereby reducing the number of occupied states near the Fermi level. (On a sidenote, this effect is not observed when the monolayer QD is deposited on BN substrate, as discussed in the next section; this could be due to the weak interaction between the QD and the substrate, as quantified below.) In addition, the atom-projected DOS of the bare bilayer QD is contrasted against that of the bare monolayer QD in Figure S4 (Supporting Information). The general trend of the plot parallels that of the monolayer QD; the most evidently disparate feature is the presence of Mo-d and S-p orbital states at around −6 eV for the bilayer QD.

The spin density distribution in the bare bilayer QD deviates to a great extent from that calculated for the bare monolayer QD (Figure 6c). The spin density is concentrated at the tail of both layers (side view), although the magnetization moment of the bilayer QD remains at 0.03 μ_B/atom.

DOI: 10.1021/jp510598x
J. Phys. Chem. C 2015, 119, 1565−1574

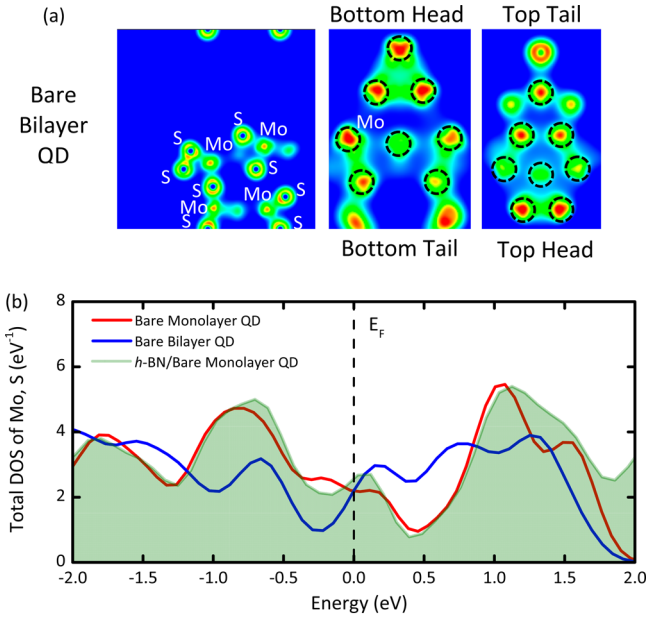

Figure 8. (a) Charge density landscape of a bare bilayer QD. The leftmost panel is the side view, and the other two panels are the top views of the layers in the QD. The black dashed circles show the position of the Mo atoms. (b) Total density of states of Mo and S atoms in bare monolayer QD, bare bilayer QD, and *h*-BN/bare monolayer QD. Zero is taken to be Fermi energy.

5. EFFECT OF BN SUBSTRATE ON MONOLAYER MoS_2 QD

The hexagonal boron nitride (*h*-BN) is generally used as a substrate for the graphene-based devices[54] because its lattice geometry is similar to graphene, and it is electrically insulating. In this section, we explore the effects of the *h*-BN substrate on the electronic properties of a triangular monolayer QD.

Figure 9 shows the side view of (a) a bare monolayer QD and (b) a fully (S) passivated monolayer QD, both of which are deposited on a *h*-BN substrate. As a prior step to depositing the QD on the substrate, the geometry of the substrate is optimized. Subsequently, the QD is added, with the Mo atom at the head of the MoS_2 QDs positioned right on top of one of the N atoms of the substrate. In the equilibrium configuration, the bare QD lies at a average distance of 3.1 Å from the substrate, while the average distance between the passivated QD and substrate is 3.7 Å (with reference to the bottom-most layer of S atoms). Note that the lattice mismatch between MoS_2 monolayer sheet and *h*-BN sheet is approximately 21%.[55] In the present case, the QD/*h*-BN heterostructure is fully optimized to partially relieve the lattice mismatch between the QD and substrate.

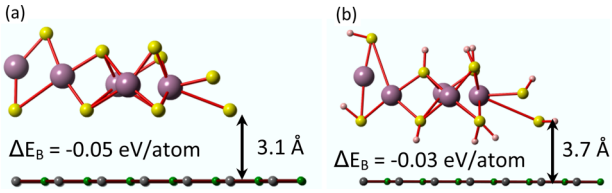

Figure 9. Side views of (a) bare monolayer QD and (b) fully (S) passivated monolayer QD, both of which are deposited on a *h*-BN substrate. The substrate−QD separation and the binding energy are shown.

The binding energy of the QD is expressed as

$$\Delta E = E_{\mathrm{MoS2/BN}} - E_{\mathrm{BN}} - E_{\mathrm{MoS2}} \quad (2)$$

where $E_{\mathrm{MoS2/BN}}$, E_{BN}, and E_{MoS2} are total energies of the QD/substrate, substrate, and the QD, respectively. The binding energy is calculated to be −0.05 and −0.03 eV/atom for the bare QD/substrate and passivated QD/substrate heterostructures, respectively. Thus, a rather weak interaction between the substrate and QD is predicted.

There is a minimal change in DOS of the QD near the Fermi level due to the *h*-BN substrate (Figure 8b). This is in stark contrast to the comparison between the monolayer and bilayer QD. For the bare QD/substrate heterostructure (Figure S5(a), Supporting Information), the occupied valence states remain relatively unchanged near the Fermi level. However, there are substantial changes to the conduction states, especially the appearance of states between 2 and 6 eV. On the other hand, for the passivated QD/substrate heterostructure, the valence states are essentially identical with or without the substrate, whereas there are subtle differences for conduction states between 2 and 4 eV (Figure S5(b), Supporting Information).

What could have contributed to the metallic nature of the bare and passivated MoS_2 QD as seen in Figures 5 and S5 (Supporting Information)? To establish the determinants, we classify the atoms by their coordination number, and plot the atom-projected DOS for the bare monolayer QD, without and with the substrate (Figure 10). It is evident that the under-coordinated edge Mo atoms predominantly contribute to the metallicity of the QD, which is retained in the presence of the substrate. This draws our attention back to the nature of the bonds in the QD, as presented earlier in Figure 4. Interestingly, metallic states appear to be localized at the under-coordinated atoms of the head and tail sections of the bare QD, although the bonds in these regions have a predominantly covalent character. This is atypical of covalent bonds, which generally form between nonmetals.

As in the case with the bare QD, the preferred spin density configuration of the QD/substrate heterostructure is predicted to be AFM (Figure 6d). The spin density distribution is primarily preserved and identical to that without the substrate (Figures 6a). This reflects the weak interaction between the QD and the substrate. In addition, the magnetization moment of the QD remains at 0.03 μ_B/atom. On the other hand, spin-up and spin-down states of the fully (S) passivated QD rearrange in a way such that the net spin density becomes negligibly small (with a maximum value of 7×10^{-8} e/Å^3) (Figure 6b).

6. ELECTRONIC TRANSPORT PROPERTIES

To investigate the electronic transport properties of QDs, we use a model setup generally employed in scanning tunneling microscopy (STM) measurements. By calculating the independent tip and sample electronic density of states, and coupling them using Tersoff−Hamann's[56] and Lang's[57] approximations to Bardeen's formulizm[58] of tunneling electrons, the tunneling characteristics and STM images can be interpreted (see the Supporting Information). This approach has been successfully applied to investigate the electronic properties of cubic PbS quantum dots and atomic wire/MoS_2 heterostructure systems.[51,59]

DOI: 10.1021/jp510598x
J. Phys. Chem. C 2015, 119, 1565−1574

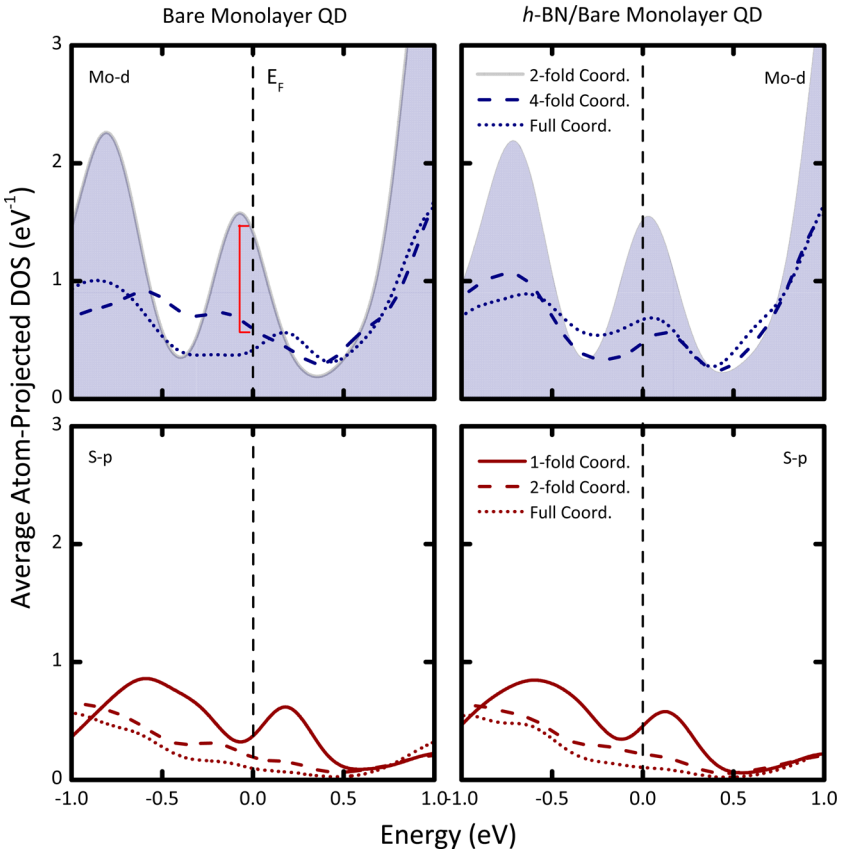

Figure 10. Calculated average atom-projected density of states of Mo (top) and S (bottom) atoms in a bare monolayer QD, and *h*-BN/bare monolayer QD, as classified by their coordination number. Zero is taken to be Fermi energy of the QD. Fully coordinated Mo and S atoms in MoS_2 have 6 and 3 nearest neighbors, respectively.

In the STM-like setup, the probe tip is positioned at a constant height of 5 Å above a central Mo atom of the QD (as marked by a black circle in Figure 1). The cap configuration of the tip is modeled by the Au_{43} cluster. The bias is defined to be positive when electrons tunnel through vacuum from the tip to the sample. Considering that the tunneling current depends exponentially on the separation between the tip and sample, the choice of this separation determines the magnitude of the tunneling current, but should not affect the predicted trend for the QDs considered.

The calculated tunneling characteristics for the low-bias voltage range of −0.2 and 0.2 V are given in Figure 11. Application of the external bias increases the current significantly for the bare QD reflecting Ohmic-like characteristics. Because the tunneling current is directly related to the convolution of the DOS of the tip and the QD, the appearance of a finite DOS at the Fermi level is associated with an increase in tunneling current with applied bias (Figure 11). However, the calculated resistance increases considerably for the bilayer QD in line with the result in Figure 8b, indicating a drastic reduction of the magnitude of the occupied states in the immediate vicinity of the Fermi level of the bilayer QD. On the other hand, the *h*-BN substrate does not have a significant effect on the total DOS of the QD near the Fermi level (Figure 8b), and hence there is minimal change to the calculated *I*−*V* characteristic of the QD/substrate heterostructure (Figure 11). The metallic states associated with the coordinatively unsaturated Mo atoms, therefore, act as conduction "channels" in MoS_2 QDs under the applied bias.

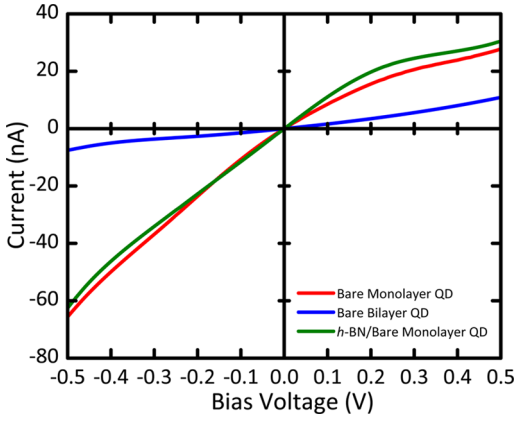

Figure 11. Calculated *I*−*V* curves of bare monolayer QD, bare bilayer QD, and QD/substrate in the constant height mode of the STM-like setup.

Next, a constant current of 1 nA, with a bias voltage of 1 V, is applied across the vacuum between the tip and the QD, as the tip is moved in the *x*−*y* plane across the QD. The triangular shape of the STM image of the bare monolayer QD (Figure 12a) and QD/substrate (Figure 12c) is distinct, while it is not clear for that of the bare bilayer QD (Figure 12b).

7. SUMMARY

Reducing the size of material to the nanometer regime introduces unusual yet interesting phenomena such as quantum size effects, which alter the properties of the material. In this

DOI: 10.1021/jp510598x
J. Phys. Chem. C 2015, 119, 1565−1574

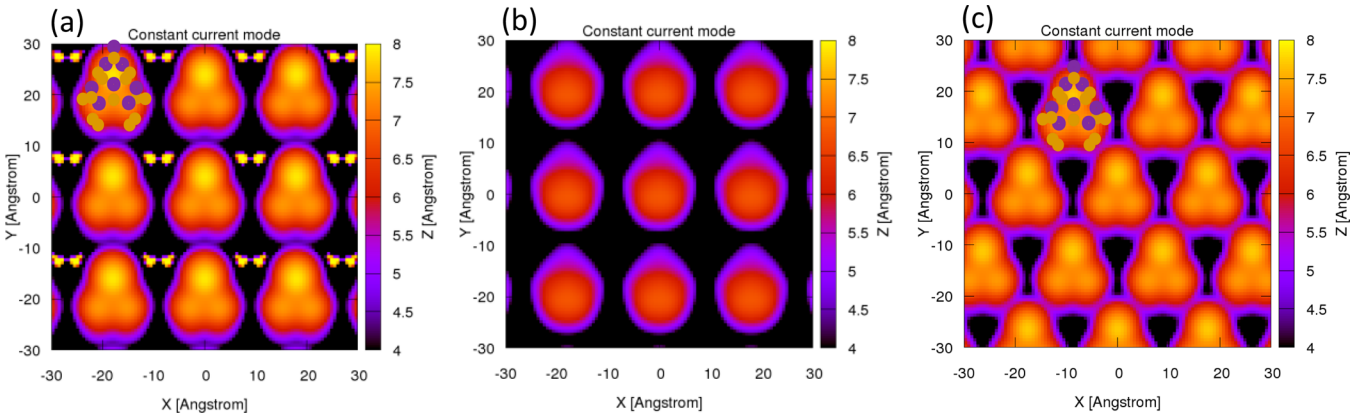

Figure 12. STM-like images in the constant current mode of (a) bare monolayer QD, (b) bare bilayer QD, and (c) QD/substrate. The orange-red regions in (a)−(c) correspond to the atomic positions in the QD, with reference to schematics of the QD atoms in (a) and (c). The color bar denotes the surface height.

study, first-principles calculations with density functional theory are employed to investigate the geometry, energetics, and electronic properties of a triangular stoichimetric QD of MoS_2. In the monolayer QD, bonding between the Mo atoms is relatively stronger than that in the monolayer sheet. This is justified by the contraction of bonds in the QD with respect to those in a monolayer MoS_2 sheet. Analysis with the quantum theory of atoms in molecules (QTAIM) shows that the Mo−S bonds are predominantly covalent at the head and tail, whereby the atoms are strongly under-coordinated, despite the presence of metallic states. This is atypical of covalent bonds, which generally form between nonmetals. Additionally, the effects of (1) edge passivation of S atoms to attenuate the quantum mechanical effects due to edge Mo atoms in the QD, (2) an additional layer (i.e., bilayer QD), and (3) a *h*-BN substrate, on the aforementioned properties of a MoS_2 QD, have been ascertained, and are presented as follows:

1. Edge Passivation. Passivating the edge S atoms modifies the geometry, energetics, and electronic characteristics of a monolayer QD, although it remains metallic. The metallic character originates from the under-coordinated Mo atoms of the QD, and is distinctly revealed by DOS. The spin density is in general uniformly distributed in the QD, but passivation redistributes the spin density, so that the spin-up states are concentrated at the head of the QD.

However, we have to note that in the context of actual synthesis of MoS_2 QDs, exposure of these samples to air might result in the termination of the coordinatively unsaturated Mo edge atoms by vapor (i.e., H_20) atoms, thereby removing the metallic states. Nevertheless, what we have presented in this study is a prediction of the behavior of these QDs in high vacuum conditions.

2. Additional Layer. The geometry, DOS, and spin density of a MoS_2 QD are found to be layer-dependent. In the bilayer, the mean distance between Mo atoms is intermediate between that of the monolayer QD and the monolayer sheet. A slightly greater structural stability of the bilayer QD could be due to the van der Waals interaction between the layers, which stabilizes the dangling bonds, and induces a large reduction in the number of occupied states near the Fermi level. In contrast to the monolayer QD, the spin density agglomerates at the tail of both top and bottom layers.

3. *h*-BN Substrate. The *h*-BN substrate has trivial effects on the electronic structure and the spin density distribution of the QD due to its weak interaction with the QD. The calculated *I*−*V* characteristics in a STM-like setup further validate preceding observations regarding the subtle modifications in the electronic structure of QD in the presence of the *h*-BN substrate.

We believe that the results of the present study are likely to extend the functionality of MoS_2-based heterostructures in catalysis and optoelectronic applications. Retention of the metallic character of the bare QD in the presence of an insulating substrate or additional layer can be influential in catalysis. Furthermore, the layer-dependent tunneling characteristics can be exploited in nanoelectronic devices.

■ ASSOCIATED CONTENT

Ⓢ Supporting Information

(A) On-site Bader charges, formation energy, intra- and interlayer bond distances; (B) chemical topology; (C) spin-polarized orbital-projected density of states − bare monolayer QD and fully (S) passivated monolayer QD; (D) atom-projected density of states − bare monolayer QD and bilayer QD; (E) atom-projected density of states − substrate-induced effects on bare monolayer QD and fully (S) passivated monolayer QD; and (F) calculations of tunneling current in a model STM-like setup. This material is available free of charge via the Internet at http://pubs.acs.org.

■ AUTHOR INFORMATION

Corresponding Authors

*E-mail: jgloh@mtu.edu.
*E-mail: pandey@mtu.edu.

Notes

The authors declare no competing financial interest.

■ ACKNOWLEDGMENTS

Funding from the following agencies is gratefully acknowledged: A*STAR International Fellowship - 2013-2015 (G.C.L.), National Science Foundation - Award Number: 1261910, Division of Materials Research (Y.K.Y.), and Army Research Laboratory - W911NF-14-2-0088 (R.P.). We thank D. R. Banyai for the STM code. The computations were performed on the MTU Superior cluster, and support from Dr. S. Gowtham is appreciated.

DOI: 10.1021/jp510598x
J. Phys. Chem. C 2015, 119, 1565−1574

REFERENCES

(1) Baugher, B. W. H.; Churchill, H. O. H.; Yang, Y.; Jarillo-Herroro, P. Intrinsic electronic transport properties of high-quality monolayer and bilayer MoS_2. *Nano Lett.* **2013**, *13*, 4212−4216.

(2) Lembke, D.; Kis, A. Breakdown of high-performance monolayer MoS_2 transistors. *ACS Nano* **2012**, *6*, 10070−10075.

(3) Ataca, C.; Şahin, H.; Aktürk, E.; Ciraci, S. Mechanical and electronic properties of MoS_2 nanoribbons and their defects. *J. Phys. Chem. C* **2011**, *115*, 3934−3941.

(4) Andriotis, A. N.; Menon, M. Tunable magnetic properties of transition metal doped MoS_2. *Phys. Rev. B* **2014**, *90*, 125304.

(5) Espejo, C.; Rangel, T.; Romero, A. H.; Gonze, X.; Rignanese, G.-M. Band structure tenability in MoS_2 under interlayer compression: A DFT and GW study. *Phys. Rev. B* **2013**, *87*, 245114.

(6) Gmelin, L., Ed. *Gmelin Handbook of Inorganic and Organometallic Chemistry*, 8th ed.; Springer-Verlag: Berlin, 1995; Vol. *B7*.

(7) Kam, K. K.; Parkinson, B. A. Detailed photocurrent spectroscopy of the semiconducting group VIB transition metal dichalcogenides. *J. Phys. Chem.* **1982**, *86*, 463−467.

(8) Doni, E.; Girlanda, R. *Electronic Structure and Electronic Transitions in Layered Materials*; Springer-Verlag: Berlin, 1986.

(9) Liu, L.; Feng, Y. P.; Shen, Z. X. Structural and electronic properties of *h*-BN. *Phys. Rev. B* **2003**, *68*, 104102.

(10) Constantinescu, G.; Kuc, A.; Heine, T. Stacking in bulk and bilayer hexagonal boron nitride. *Phys. Rev. Lett.* **2013**, *111*, 036104.

(11) Mak, K. F.; He, K. L.; Shan, J.; Heinz, T. F. Control of valley polarization in monolayer MoS_2 by optical helicity. *Nat. Nanotechnol.* **2012**, *7*, 494−498.

(12) Rycerz, A.; Tworzydlo, J.; Beenakker, C. W. J. Valley filter and valley valve in graphene. *Nat. Phys.* **2007**, *3*, 172−175.

(13) Novoselov, K. S.; Jiang, D.; Schedin, F.; Booth, T. J.; Khotkevich, V. V.; Morozov, S. V.; Geim, A. K. Two-dimensional atomic crystals. *Proc. Natl. Acad. Sci. U.S.A.* **2005**, *102*, 10451−10453.

(14) Lee, Y.-H.; Zhang, X.-Q.; Zhang, W.; Chang, M.-T.; Lin, C.-T.; Chang, K.-D.; Yu, Y.-C.; Wang, J. T. -W.; Chang, C.-S.; Li, L.-J.; et al. Synthesis of large-area MoS_2 atomic layers with chemical vapor deposition. *Adv. Mater.* **2012**, *24*, 2320−2325.

(15) Van der Zande, A. M.; Huang, P. Y.; Chenet, D. A.; Berkelbach, T. C.; You, Y.; Lee, G.-H.; Heinz, T. F.; Reichman, D. R.; Muller, D. A.; Hone, J. C. Grains and grain boundaries in highly crystalline monolayer molybdenum disulphide. *Nat. Mater.* **2013**, *12*, 554−561.

(16) Najmaei, S.; Liu, Z.; Zhou, W.; Zou, X.; Shi, G.; Lei, S.; Yakobson, B. I.; Idrobo, J.-C.; Ajayan, P. M.; Lou, J. Vapour phase growth and grain boundary structure of molybdenum disulphide atomic layers. *Nat. Mater.* **2013**, *12*, 754−759.

(17) Wang, H.; Yu, L.; Lee, Y.-H.; Fang, W.; Hsu, A.; Herring, P.; Chin, M.; Dubey, M.; Li, L.-J.; Kong, J.; et al. Large-scale 2D electronics based on single-layer MoS_2 grown by chemical vapor deposition. *IEEE Int. Electron Devices Meeting*, 2012, 4.6.1.

(18) Wu, W.; De, D.; Chang, S.-C.; Wang, Y.; Peng, H.; Bao, J.; Pei, S.-S. High mobility and high on/off ratio field-effect transistors based on chemical vapor deposited single-crystal MoS_2 grains. *Appl. Phys. Lett.* **2013**, *102*, 142106.

(19) Zhou, W.; Zou, X. L.; Najmaei, S.; Liu, Z.; Shi, Y. M.; Kong, J.; Lou, J.; Ajayan, P. M.; Yakobson, B. I.; Idrobo, J. C. Intrinsic structural defects in monolayer molybdenum disulfide. *Nano Lett.* **2013**, *13*, 2615−2622.

(20) Mann, J.; Sun, D. Z.; Ma, Q.; Chen, J. R.; Preciado, E.; Ohta, T.; Diaconescu, B.; Yamaguchi, K.; Tran, T.; Wurch, M.; et al. Facile growth of monolayer MoS_2 film areas on SiO_2. *Eur. Phys. J. B* **2013**, *86*, 226.

(21) Schmidt, H.; Wang, S.; Chu, L.; Toh, M.; Kumar, R.; Zhao, W.; Castro Neto, A. H.; Martin, J.; Adam, S.; Özyilmaz, B.; et al. Transport properties of monolayer MoS_2 grown by chemical vapor deposition. *Nano Lett.* **2014**, *14*, 1909−1913.

(22) Sorensen, S. G.; Füchtbauer, H. G.; Tuxen, A. K.; Walton, A. S.; Lauritsen, J. V. Structure and electronic properties of in situ synthesized single-layer MoS_2 on a gold surface. *ACS Nano* **2014**, *8*, 6788−6796.

(23) Bertram, N.; Cordes, J.; Kim, Y.; Gantefo, G.; Gemming, S.; Seifert, G. Nanoplatelets made from MoS_2 and WS_2. *Chem. Phys. Lett.* **2006**, *418*, 36−39.

(24) Helveg, S.; Lauritsen, J. V.; Lagsgaard, E.; Stensgaard, I.; Norskov, J. K.; Clausen, B. S.; Topsoe, H.; Besenbacher, F. Atomic-scale structure of single-layer MoS_2 nanoclusters. *Phys. Rev. Lett.* **2000**, *84*, 951.

(25) Lauritsen, J. V.; Kibsgaard, J.; Helveg, S.; Topsoe, H.; Clausen, B.; Lagsgaard, E.; Besenbacher, F. Size-dependent structure of MoS_2 nanocrystals. *Nat. Nanotechnol.* **2007**, *2*, 53−58.

(26) Seifert, G.; Tamuliene, J.; Gemming, S. Mo_nS_{2n+x} clusters − Magic numbers and platelets. *Comput. Mater. Sci.* **2006**, *35*, 316−320.

(27) Berger, C.; Song, Z.; Li, X.; Wu, X.; Brown, N.; Naud, C.; Mayou, D.; Li, T.; Hass, J.; Marchenkov, A. N.; et al. Electronic confinement and coherence in patterned epitaxial graphene. *Science* **2006**, *312*, 1191−1196.

(28) Lin, Y.-C.; Dumcenco, D. O.; Huang, Y.-S.; Suenaga, K. Atomic mechanism of the semiconducting-to-metallic phase transition in single-layered MoS_2. *Nat. Nanotechnol.* **2014**, *9*, 391−396.

(29) Nayak, A. P.; Bhattacharyya, S.; Zhu, J.; Liu, J.; Wu, X.; Pandey, T.; Jin, C.; Singh, A. K.; Akinwande, D.; Lin, J. F. Pressure-induced semiconducting to metallic transition in multilayered molybdenum disulphide. *Nat. Commun.* **2014**, *5*, 3731.

(30) Lauritsen, J. V.; Nyberg, M.; Vang, R. T.; Bollinger, M. V.; Clausen, B. S.; Topsoe, H.; Jacobsen, K. W.; Lægsgaard, E.; Norskov, J. K.; Besenbacher, F. Chemistry of one-dimensional metallic edge states in MoS_2 nanoclusters. *Nanotechnology* **2003**, *14*, 385−389.

(31) Bollinger, M. V.; Jacobsen, K. W.; Norskov, J. K. Atomic and electronic structure of MoS_2 nanoparticles. *Phys. Rev. B* **2003**, *67*, 085410.

(32) Bader, R. F. W. *Atoms in Molecules. A Quantum Theory*; Clarendon Press: Oxford, 1994.

(33) Bader, R. F. W. Atoms in molecules. *Acc. Chem. Res.* **1985**, *18*, 9−15.

(34) Bader, R. F. W. A quantum theory of molecular structure and its applications. *Chem. Rev.* **1991**, *91*, 893−928.

(35) Sagar, R. P.; Ku, A. C. T.; Smith, V. H., Jr.; Simas, A. M. The Laplacian of the charge density and its relationship to the shell structure of atoms and ions. *J. Chem. Phys.* **1988**, *88*, 4367.

(36) Shi, Z.; Boyd, R. J. The shell structure of atoms and the Laplacian of the charge density. *J. Chem. Phys.* **1988**, *88*, 4375.

(37) Cowley, J. M.; Moodie, A. F. The scattering of electrons by atoms and crystals. I. A new theoretical approach. *Acta Crystallogr.* **1957**, *10*, 609−619.

(38) Kirkland, E. J. *Advanced Computing in Electron Microscopy*, 2nd ed.; Springer: New York, 2010.

(39) Kresse, G.; Joubert, D. From ultrasoft pseudopotentials to the projector augmented-wave method. *Phys. Rev. B* **1999**, *59*, 1758.

(40) Perdew, J. P.; Burke, K.; Ernzerhof, M. Generalized gradient approximation made simple. *Phys. Rev. Lett.* **1996**, *77*, 3865.

(41) Grimme, S. Semiempirical GGA-type density functional constructed with a long-range dispersion correction. *J. Comput. Chem.* **2006**, *27*, 1787−1799.

(42) Monkhorst, H. J.; Pack, J. D. Special points for Brillouin-zone integrations. *Phys. Rev. B* **1976**, *13*, 5188.

(43) Hellmann, H. *Einführung in die quantenchemie*; Leipzig, 1937.

(44) Feynman, R. P. Forces in molecules. *Phys. Rev.* **1939**, *56*, 340.

(45) Kiguchi, M.; Takai, K.; Joseph Joly, V. L.; Enoki, T.; Sumii, R.; Amemiya, K. Magnetic edge state and dangling bond state of nanographene in activated carbon fibers. *Phys. Rev. B* **2011**, *84*, 045421.

(46) Topsoe, N. Y.; Topsoe, H. FTIR studies of Mo/Al_2O_3-based catalysts: II. Evidence for the presence of SH groups and their role in acidity and activity. *J. Catal.* **1993**, *139*, 641−651.

(47) Sun, C. Q. Size dependence of nanostructures: impact of bond order deficiency. *Prog. Solid State Chem.* **2007**, *35*, 1−159.

(48) Pauling, L. Atomic radii and interatomic distances in metals. *J. Am. Chem. Soc.* **1947**, *69*, 542−553.

(49) Goldschmidt, V. M. *Ber. Dtsch. Chem. Ges.* **1927**, *60*, 1270.

DOI: 10.1021/jp510598x
J. Phys. Chem. C 2015, 119, 1565−1574

(50) Pauling, L. The nature of the chemical bond. IV. The energy of single bonds and the relative electronegativity of atoms. *J. Am. Chem. Soc.* **1932**, *54*, 3570−3582.
(51) Kumar, A.; Banyai, D.; Ahluwalia, P. K.; Pandey, R.; Karna, S. P. Electronic stability and Electron transport properties of atomic wires anchored on the MoS_2 monolayer. *Phys. Chem. Chem. Phys.* **2014**, *16*, 20157−20163.
(52) Wang, Z. L.; Hui, C. Z. *Electron Microscopy of Nanotubes*; Tsinghua University Press: Beijing, China, 1991.
(53) Bartlett, G. J.; Newberry, R. W.; VanVeller, B.; Raines, R. T.; Woolfson, D. N. Interplay of hydrogen bonds and n→π^* in proteins. *J. Am. Chem. Soc.* **2013**, *135*, 18682−18688.
(54) Dean, C. R.; Young, A. F.; Meric, I.; Lee, C.; Wang, L.; Sorgenfrei, S.; Watanabe, K.; Taniguchi, T.; Kim, P.; Shepard, K. L.; et al. Boron nitride substrates for high-quality graphene electronics. *Nat. Nanotechnol.* **2010**, *5*, 722−726.
(55) Huang, Z.; He, C.; Qi, X.; Yang, H.; Liu, W.; Wei, X.; Peng, X.; Zhong, J. Band structure engineering of monolayer MoS_2 on *h*-BN: first-principles calculations. *J. Phys. D: Appl. Phys.* **2014**, *47*, 075301.
(56) Tersoff, J.; Hamann, D. R. Theory and application for the scanning tunnelling microscope. *Phys. Rev. Lett.* **1983**, *50*, 1998.
(57) Lang, N. D. Spectroscopy of single atoms in the scanning tunnelling microscope. *Phys. Rev. B* **1986**, *34*, 5947.
(58) Bardeen, J. Tunneling from a many-particle point of view. *Phys. Rev. Lett.* **1961**, *6*, 57.
(59) Gupta, S. K.; He, H.; Banyai, D. R.; Kandalam, A. K.; Pandey, R. Electron tunneling characteristics of a cubic quantum dot. *J. Chem. Phys.* **2013**, *139*, 244307.

DOI: 10.1021/jp510598x
J. Phys. Chem. C 2015, 119, 1565−1574

Supporting Information

For

MoS_2 Quantum Dots: Effects of Passivation, Additional Layer, and *h*-BN Substrate on the Stability and Electronic Properties

G.C. Loh [a,b*], Ravindra Pandey [a,*], Yoke Khin Yap [a] and Shashi P. Karna [c]

[a]Department of Physics, Michigan Technological University, Houghton, Michigan 49931, USA
[b]Institute of High Performance Computing, 1 Fusionopolis Way, #16-16 Connexis, Singapore 138632
[c]US Army Research Laboratory, Weapons and Materials Research Directorate, ATTN: RDRL-WM, Aberdeen Proving Ground, MD 21005-5069, U.S.A.

A. On-site Bader Charges, Formation Energy, Intra- and Inter-layer Bond Distances

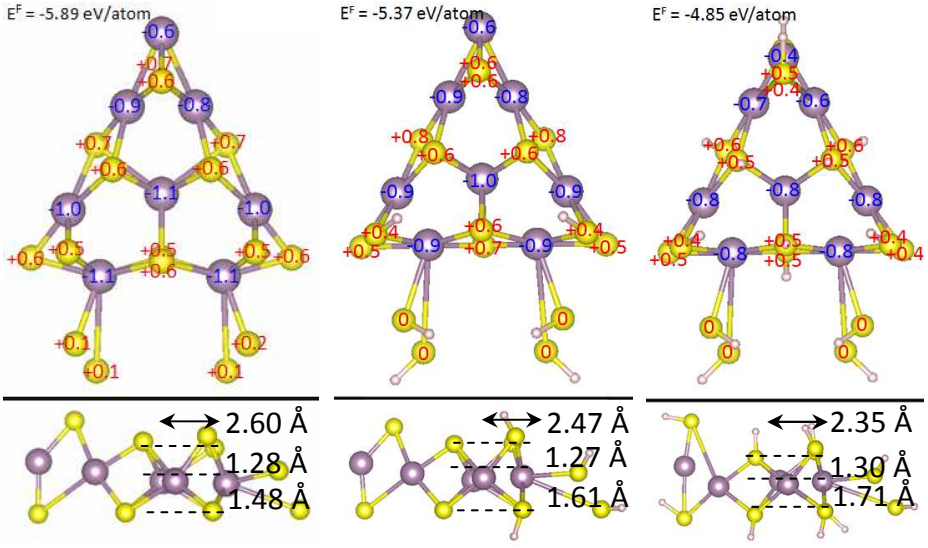

Figure S1. Top and side views of bare monolayer QD, partially (S) passivated monolayer QD, and fully (S) passivated monolayer QD: On-site Bader charges, formation energy, intra- and inter-layer bond distances.

B. Chemical Topology

Apart from the Laplacian of the electron density, the chemical bond can also be described accurately by the electron localization function (ELF) [1-3]. In this study, we utilise the electron density with Bader's quantum theory of atoms in molecules [4-6] to analyse the chemical topology of the MoS_2 QD.

Mathematically, the Laplacian operator is a second derivative or the trace of the Hessian of a function; it denotes the local minimum/maximum, or in other words, the saddle point of that function. Both minimum and maximum points are *critical points* at which the first derivatives of the function become zero. In the context of chemical topology, the differential operator reproduces the spherical shell structure of isolated atoms by alternating shells of charge concentration and shells of charge depletion [7,8]. The outermost shell of charge concentration of an atom is called the valence shell charge concentration (VSCC), and its spherical symmetry is broken when the atom bonds with another atom. Another feature in the Laplacian plot of the electron density is the nuclear critical point (NCP), which is a local maximum in electron density, and is located at the position of a nucleus. A zero-flux surface contains a set of Laplacian trajectories which terminate at the bond critical point (bcp) where the Laplacian equals zero.

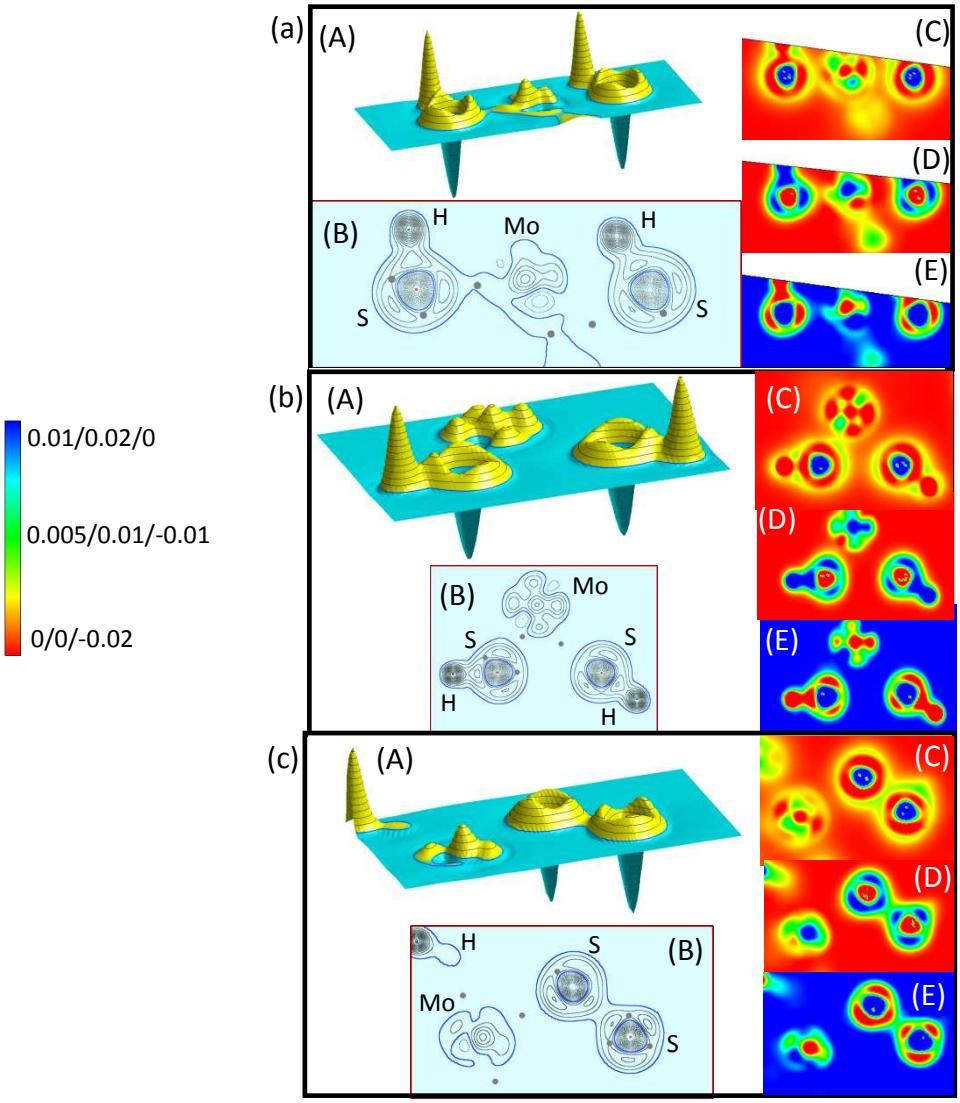
0.01/0.02/0
0.005/0.01/-0.01
0/0/-0.02
(a)
(A)
(B)
H
Mo
H
S
S
(C)
(D)
(E)
(b)
(A)
(B)
Mo
S
S
H
H
(C)
(D)
(E)
(c)
(A)
(B)
H
S
Mo
S
(C)
(D)
(E)

Figure S2. Passivated MoS_2 QD: (A) 3D negative Laplacian plot, (B) 2D negative Laplacian plot, (C) kinetic energy density, (D) potential energy density, and (E) electronic energy density of (a) head, (b) mid-section, (c) tail. The green and red lines in the 2D negative Laplacian plots represent the maxima and minima of electron density, respectively. The color bar shows the energy density in $E_h a_0^{-3}$, whereby E_h is hartree and a_0 is Bohr radius, with the numerals in the scale for the kinetic, potential, and electronic energy densities, respectively.

C. Spin-Polarized Orbital-Projected Density of States - Bare Monolayer QD and Fully (S) Passivated Monolayer QD

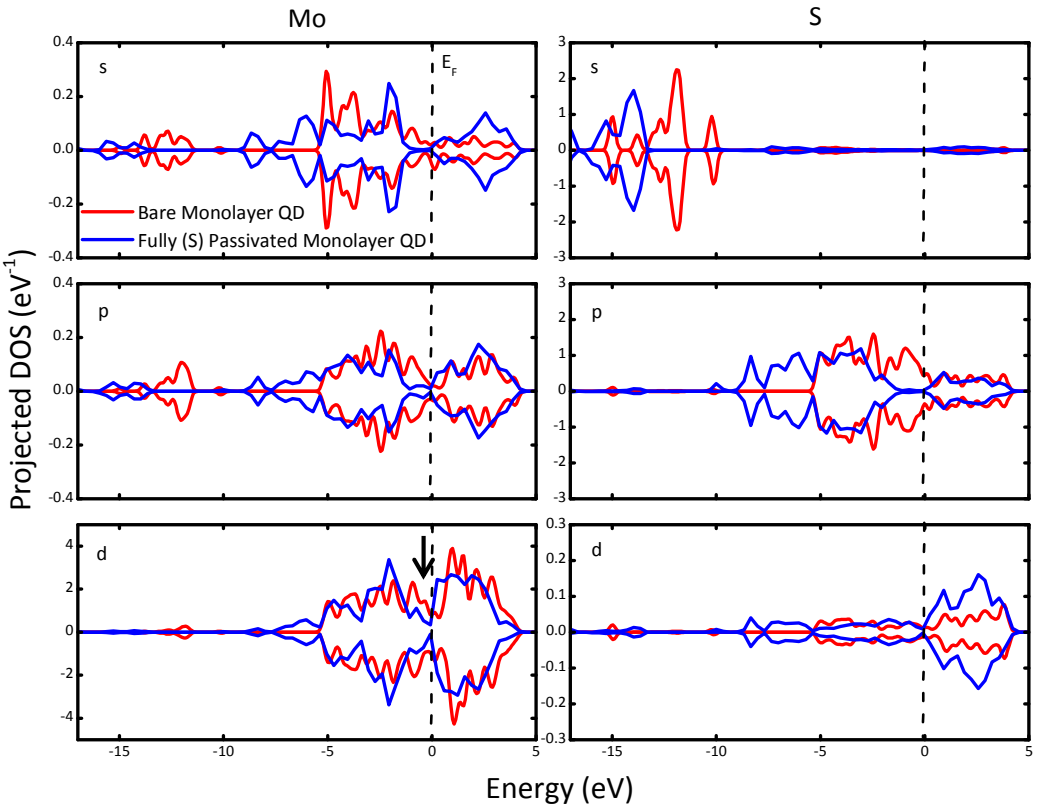

Figure S3. Spin-polarized orbital-projected density of states of Mo and S atoms in the bare monolayer QD and fully (S) passivated monolayer QD.

D. Atom-Projected Density of States - Bare Monolayer QD and Bilayer QD

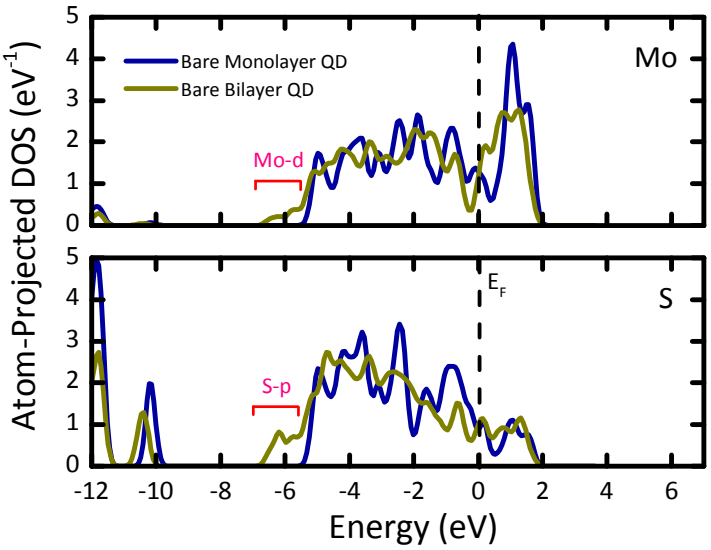

Figure S4. Atom-projected density of states of bare monolayer QD and bilayer QD. Zero is taken to be Fermi energy of the QD.

E. Atom-Projected Density of States – Substrate-induced Effects on Bare Monolayer QD and Fully (S) Passivated Monolayer QD

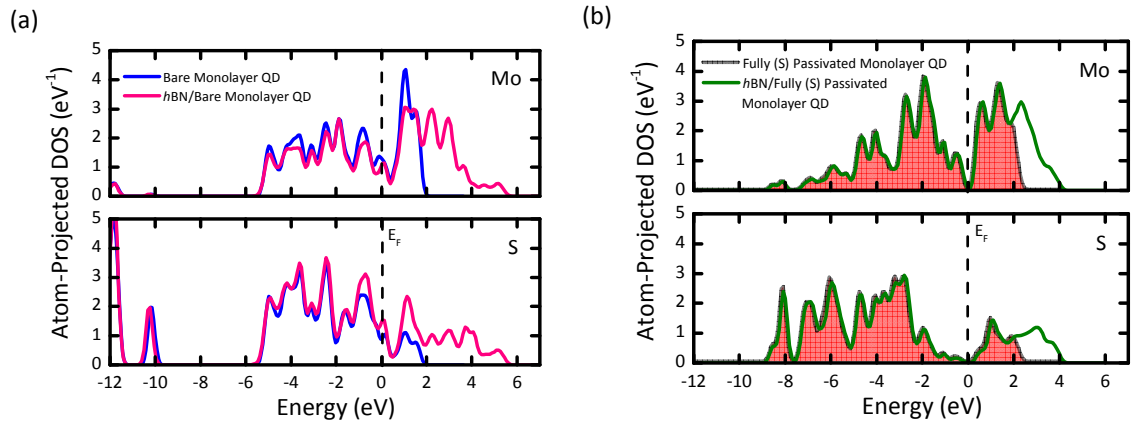

Figure S5. Atom-projected density of states of (a) bare monolayer QD, and (b) fully (S) passivated monolayer QD without and with h-BN substrate. Zero is taken to be Fermi energy of the QD.

F. Calculations of Tunneling Current in a Model STM-like Setup

Scanning tunneling microscopy (STM) has been widely used to image surfaces at the atomic level. By calculating the independent tip and sample electronic density of states, and coupling them using Tersoff-Hamann's [9] and Lang's [10] approximations to Bardeen's formulism [11] of tunneling electrons, the STM images can be accurately interpreted. In this approach, at a low-bias limit, the STM probing tip is assumed to have one active s-like orbital in the apex atom [9].

The electron tunneling current for both spin-up and spin-down states are computed separately in the expression [12].

$$I^{\uparrow(\downarrow)} = \frac{2\pi e}{\hbar} \int_{-eV/e}^{eV/2} \rho_s^{\uparrow(\downarrow)}\left(\varepsilon + \frac{eV}{2}\right) \rho_t^{\uparrow(\downarrow)}\left(\varepsilon - \frac{eV}{2}\right) \times e^{-2d\sqrt{2\left(\frac{m_e}{\hbar^2}\right)(\varphi_{av}-\varepsilon)}} \left\{\left[f\left(\varepsilon - \frac{eV}{2}\right)\right]\left[1 - f\left(\varepsilon + \frac{eV}{2}\right)\right] - \left[f\left(\varepsilon + \frac{eV}{2}\right)\right]\left[1 - f\left(\varepsilon - \frac{eV}{2}\right)\right]\right\} d\varepsilon \quad (1)$$

where $\rho_s^{\uparrow(\downarrow)}$ and $\rho_t^{\uparrow(\downarrow)}$ are the spin-up (and spin-down) projected densities of states of the tip and sample, respectively, d is the sample-tip distance, ε is the injection energy of the tunnelling electron, e is the electronic charge, m_e is the electron effective mass, $\hbar$ is the reduced Planck constant, φ_{av} is the average work function of the sample and the tip, and f is the Fermi-Dirac distribution function. Under a low-bias, the electron effective mass (m_e) and average work function (φ_{av}) are assumed to be constant.

REFERENCES

(1) Savin, A.; Nesper, R.; Wengert, S.; Fässler, T. F. ELF: The electron localization function. *Angew. Chem. Int. Ed. Engl.* **1997**, *36*, 1808-1832.

(2) Poater, J.; Duran, M.; Solà, M.; Silvi, B. Theoretical evaluation of electron delocalization in aromatic molecules by means of atoms in molecules (AIM) and electron localization function (ELF) topological approaches. *Chem. Rev.* **2005**, *105*, 3911-3947.

(3) Alikhani, M. E.; Fuster, F.; Silvi, B. What can tell the topological analysis of ELF on hydrogen bonding. *Structural Chem.* **2005**, *16*, 203-210.

(4) Berger, C.; Song, Z.; Li, X.; Wu, X.; Brown, N.; Naud, C.; Mayou, D.; Li, T.; Hass, J.; Marchenkov, A. N et al. Electronic confinement and coherence in patterned epitaxial graphene. *Science* **2006**, *312*, 1191-1196.

(5) Bader, R. F. W. *Atoms in molecules. A quantum theory*; Clarendon Press: Oxford, 1994.

(6) Bader, R. F. W. Atoms in molecules. *Acc. Chem. Res.* **1985**, *18*, 9-15.

(7) Sagar, R. P.; Ku, A. C. T.; Smith, V. H. Jr.; Simas, A. M. The Laplacian of the charge density and its relationship to the shell structure of atoms and ions. *J. Chem. Phys.* **1988**, *88*, 4367.

(8) Shi, Z.; Boyd, R. J. The shell structure of atoms and the Laplacian of the charge density. *J. Chem. Phys.* **1988**, *88*, 4375.

(9) Tersoff, J.; Hamann, D. R. Theory and application for the scanning tunnelling microscope. *Phys. Rev. Lett.* **1983**, *50*, 1998.)

(10) Lang, N. D. Spectroscopy of single atoms in the scanning tunnelling microscope. *Phys. Rev. B* **1986**, *34*, 5947.

(11) Bardeen, J. Tunneling from a many-particle point of view. *Phys. Rev. Lett.* **1961**, *6*, 57.

(12) He, H.; Pandey, R.; Pati, R.; Karna, S. P. Spin-polarized electron transport of a self-assembled organic monolayer on a Ni(111) substrate: An organic spin switch. *Phys. Rev. B* **2006**, *73*, 195311.